



Article

Machine Learning and Deep Learning-Based Atmospheric Duct Interference Detection and Mitigation in TD-LTE Networks [†]

Rasendram Muralitharan ¹, Upul Jayasinghe ¹, Roshan G. Ragel ¹ and Gyu Myoung Lee ^{2,*}

¹ Department of Computer Engineering, Faculty of Engineering, University of Peradeniya, Peradeniya 20400, Sri Lanka; murali90@eng.jfn.ac.lk (R.M.); upuljm@eng.pdn.ac.lk (U.J.); roshanr@eng.pdn.ac.lk (R.G.R.)

² Faculty of Engineering and Technology, Liverpool John Moores University, Liverpool L3 3AF, UK

* Correspondence: g.m.lee@ljmu.ac.uk

[†] The manuscript is the extended version of the conference paper: Muralitharan, R.; Jayasinghe, U.; Ragel, R.G. Machine Learning based Atmospheric Duct Interference Evaluation in TD-LTE Networks. In Proceedings of the 2023 IEEE 17th International Conference on Industrial and Information Systems (ICIIS), Peradeniya, Sri Lanka, 25–26 August 2023; pp. 377–382, <https://doi.org/10.1109/ICIIS58898.2023.10253504>.

Abstract: The variations in the atmospheric refractivity in the lower atmosphere create a natural phenomenon known as atmospheric ducts. The atmospheric ducts allow radio signals to travel long distances. This can adversely affect telecommunication systems, as cells with similar frequencies can interfere with each other due to frequency reuse, which is intended to optimize resource allocation. Thus, the downlink signals of one base station will travel a long distance via the atmospheric duct and interfere with the uplink signals of another base station. This scenario is known as atmospheric duct interference (ADI). ADI could be mitigated using digital signal processing, machine learning, and hybrid approaches. To address this challenge, we explore machine learning and deep learning techniques for ADI prediction and mitigation in Time-Division Long-Term Evolution (TD-LTE) networks. Our results show that the Random Forest algorithm achieves the highest prediction accuracy, while a convolutional neural network demonstrates the best mitigation performance with accuracy. Additionally, we propose optimizing special subframe configurations in TD-LTE networks using machine learning-based methods to effectively reduce ADI.

Keywords: TD-LTE; ADI; machine learning; SVM; random forest; LSTM; CNN



Academic Editors: Demetris Trihinas and Alexandros Karakasidis

Received: 21 April 2025

Revised: 19 May 2025

Accepted: 21 May 2025

Published: 27 May 2025

Citation: Muralitharan, R.; Jayasinghe, U.; Ragel, R.G.; Lee, G.M. Machine Learning and Deep Learning-Based Atmospheric Duct Interference Detection and Mitigation in TD-LTE Networks. *Future Internet* **2025**, *17*, 237. <https://doi.org/10.3390/fi17060237>

Copyright: © 2025 by the authors. Licensee MDPI, Basel, Switzerland. This article is an open access article distributed under the terms and conditions of the Creative Commons Attribution (CC BY) license (<https://creativecommons.org/licenses/by/4.0/>).

1. Introduction

Variations in atmospheric weather conditions in the low atmosphere cause changes in atmospheric refractivity. These changes create a phenomenon known as atmospheric ducts in the lower atmosphere. The atmospheric duct allows radio frequency signals to travel long distances. Mobile signals could travel through atmospheric ducts and reach large propagation distances. The mobile operators use a frequency reuse pattern among the cells to increase the spectral efficiency of the mobile networks. Atmospheric duct interference (ADI) occurs when downlink mobile signals from one base station propagate over long distances through atmospheric ducts and disrupt the uplink mobile signals of another base station with the same frequency [1,2]. The formation of the atmospheric duct depends on the weather conditions, such as atmospheric temperature, atmospheric pressure, and atmospheric humidity [3]. The length of the atmospheric duct will vary from 100 km to 400 km, depending on the atmospheric conditions. We can classify the atmospheric duct into three classes, surface duct, elevated duct, and evaporation duct, based on the characteristics of the atmospheric ducts in the lower atmosphere [4,5].

Mitigating ADI is crucial for enhancing the quality of service (QoS) in mobile networks and maintaining reliable service level agreements. While traditional signal processing techniques have been employed, machine learning and hybrid approaches offer more efficient solutions. This study explores the relationship between uplink power, weather conditions, and uplink interference in physical resource blocks (PRBs) within 4G Long-Term Evolution (LTE) networks. By analyzing samples of network data and corresponding weather data, we demonstrate how machine learning models can effectively detect ADI and help optimize guard period adjustments. However, modifying the guard period may lead to frequency overlap with adjacent base stations, making precise synchronization of uplink and downlink signals essential for effective ADI mitigation [2,6].

Our research focuses on developing a machine learning-based ADI prediction and mitigation system for Time-Division Long-Term Evolution (TD-LTE) networks. The proposed models incorporate both atmospheric and network-related features to enhance accuracy. Specifically, we utilize three atmospheric parameters—temperature, humidity, and pressure—alongside fifteen network-side features obtained from the mobile operator. All features are normalized between 0 and 1 for consistency. Atmospheric data are sourced from the Visual Crossing weather monitoring platform, while network data are collected from Dialog Axiata PLC in Sri Lanka [7]. The dataset spans two years, covering 2021 to 2023, with 56,000 entries collected from the Jaffna district.

For ADI prediction, we implement four machine learning algorithms: Support Vector Machine (SVM), Random Forest, Long Short-Term Memory (LSTM), and a convolutional neural network (CNN). Among these, the Random Forest model achieves the highest test accuracy of 72.3%. For ADI mitigation, we employ five classifiers: Stochastic Gradient Descent, Gradient Boosting, Optimized Distributed Gradient Boosting, LSTM, and a CNN, with the CNN delivering the best performance at 75% accuracy. In TD-LTE networks, the time interval between uplink and downlink frames is managed through special subframes, consisting of an uplink pilot time slot, a downlink pilot time slot, and a guard period. Our mitigation strategy dynamically configures the guard period based on machine learning predictions to minimize ADI while ensuring seamless network synchronization [8,9].

We are unable to collect the inter-cell and intra-cell interference values at the receiver side. If we consider the values in the features of the models, then we can improve the performance of the models.

This paper is structured into seven sections. The first section provides an introduction to the research, outlining its objectives and significance. The second section presents a review of related work, highlighting existing studies and methodologies relevant to ADI mitigation. The third section details the research methodology, including data collection, feature selection, and model development. The fourth section discusses the results and findings, offering an in-depth analysis and interpretation of the outcomes. The fifth section presents the conclusions derived from this study. The sixth section outlines potential directions for future research. Finally, the seventh section includes acknowledgments.

2. Related Works

Atmospheric duct interference (ADI) poses a substantial challenge to the performance, coverage, and quality of service in contemporary wireless communication systems, particularly in TD-LTE and 5G Radio networks. To address these issues, a diverse body of research has explored various ADI detection and mitigation techniques. Existing studies have analyzed signal processing-based methods, machine learning and deep learning frameworks, hybrid algorithmic strategies, and simulation-based evaluations. Each of these methodologies contributes valuable insights into the nature of ADI and the effectiveness of different mitigation strategies under realistic deployment conditions.

The following subsections review the key contributions within each of these methodological categories. By analyzing the strengths, limitations, and empirical results of the proposed approaches, we aim to identify existing research gaps and motivate the development of more robust and adaptive interference mitigation systems suitable for next-generation wireless networks.

2.1. Signal Processing Approach to Mitigate ADI

Peralta et al. [10] have developed an atmospheric duct interference mitigation system for the 5G New Radio mobile networks. The 5G New Radio mobile network uses an orthogonal frequency division multiplication scheme to multiplex the information-bearing signals in the carrier signals. The mitigation scheme uses remote interference management-based reference signal design to recognize and mitigate the atmospheric duct interference in 5G New Radio mobile networks. The reference signals are placed in two carrier types: Additive White Gaussian Noise (AWGN) and tapped-delay line (TDL-E). The false alarm rate and detection probabilities are plotted with different Signal-to-Noise ratios in the experiments.

Also, Peralta et al. [8] published another article, which also used remote interference reference signal sequences to detect atmospheric duct interference in the 5G New Radio networks. They designed the 5G New Radio system in AWGN and TDL-E channels. The comb 1 and 2 systems achieved an 18 dB Signal-to-Noise Ratio (SNR), and the comb 4 system achieved a 13 dB SNR.

Guo et al. [11] developed an ADI mitigation system that can adjust the guard period based on the remote interference reference signal in 5G New Radio. They have obtained a 5–7 dB SNR reduction in 5G New Radio networks.

Shen et al. [12] used the ADI mitigation systems in TD-LTE networks. The mitigation approaches were developed based on the decisions of the TD-LTE reference signals. They used three different ADI mitigation approaches. The first approach was developed by controlling the signal power of the antenna. The second approach was developed by controlling the elevation angle of the antenna. The third approach controlled the antenna height.

The referenced studies highlight that atmospheric ducting significantly exacerbates interference, particularly in lower frequency bands (sub-6 GHz) due to their superior long-distance propagation characteristics. Consequently, the majority of the literature on 5G New Radio (NR) focuses on Frequency Range 1 (FR1, 410 MHz–7.125 GHz) compared to Frequency Range 2 (FR2, 24.25–71 GHz), as FR1 bands are more susceptible to such interference phenomena.

A summary of the digital signal processing-based mitigation schemes is given in Table 1.

Table 1. Digital signal processing-based mitigation approaches.

Approach	Year	Detection Methodology	Accuracy	Network
Peralta et al. [10]	2019	Fast Fourier transform	Detection probability: 0.900 False alarm probability: 0.002	5G New Radio (FR1)
Peralta et al. [8]	2021	Remote interference reference signal design	18 dB SNR for comb 1 and 2, 13 dB SNR for comb 4.	5G New Radio (FR1 and FR2)
Guo et al. [11]	2024	Guard period adjustment based on remote interference	5–7 dB SNR reduction	5G New Radio (FR1 and FR2)
Shen et al. [12]	2017	ADI mitigation systems based on the TD-LTE reference signals	Power: 1–2 dB SNR reduction, Elevation angle: 5–10 dB SNR reduction, Antenna height: 3–4 dB SNR reduction	TD-LTE Networks

2.2. Machine Learning and Deep Learning Approaches to Mitigate ADI

Zhou et al. [3] developed a machine learning model to predict and mitigate the atmospheric duct interference in the TD-LTE networks. They utilized a framework called alternating direction methods of multiplier to predict and mitigate the atmospheric duct interference in the TD-LTE networks. The framework uses a linear distributed Support Vector Machine (SVM) algorithm. The machine learning model uses meteorological and network-side datasets. The two datasets are converted to an interference map in the preprocessing stage. The meteorological dataset is collected from a radiosonde in Baoshan city in Shanghai province in China, and the network-side dataset is collected from the China Mobile operator. Kriging interpolation is used in the preprocessing stage. The variations in the modified refractivity in the low atmosphere are the major reason for the formation of the atmospheric ducts.

Ren et al. [13] developed an atmospheric duct interference mitigation system using convolutional neural networks. The network-side dataset is collected from the Shenzhen division primary carrier in a province in China. The convolutional neural network model contains three convolutional layers and two fully connected layers. The network-side dataset contains interference data from the Global System for Mobile Communications (GSM), Digital Enhanced Cordless Telephone, and TD-LTE networks. The spectral waterfall images are generated from the power spectral density plot and the time domain plot. The time value is plotted on the *x*-axis, and the frequency value is plotted on the *y*-axis. The test dataset of the mitigation system is collected from 10,000 TD-LTE network cells in a province in China. The experiment is performed for eight different cases.

Sun et al. [14] developed an atmospheric duct interference prediction system using machine learning approaches in the TD-LTE networks. The prediction system uses the Support Vector Machine, Random Forest, and K-Nearest Neighbor algorithms. The key idea of learning a decision tree is how to choose the optimal division attribute. This study used a Classification and Regression Tree (CART) decision tree in the Random Forest algorithm to predict the atmospheric duct interference in the TD-LTE networks. The CART decision tree applies the Gini index to select the optimal division attributes. The interference dataset is converted to an interference map. The network-side dataset is collected from the China Mobile operator. The atmospheric side data are collected from a radiosonde in a province in China. The run-time values of the different mitigation systems are compared in this research paper.

A summary of the machine learning- and deep learning-based mitigation systems is given in Table 2.

Table 2. The machine learning- and deep learning-based approaches.

Approach	Year	Detection Methodology	Train Accuracy	Test Accuracy	Network
Ren et al. [13]	2019	CNN	-	0.856	LTE/Wi-Fi
Sun et al. [14]	2017	Random Forest	-	0.650 (4000 samples), 0.680 (10,000 samples), 0.700 (20,000 samples)	TD-LTE
Shen et al. [15]	2020	CNN	0.990	0.977	TD-LTE
Zhou et al. [3]	2017	SVM KNN	-	0.680 (10,000 samples), 0.720 (40,000 samples) 2. 0.700 (10,000 samples), 0.710 (40,000 samples)	TD-LTE
Yang et al. [16]	2021	LSTM	-	0.984	5G (FR1)

2.3. Hybrid Approaches to Mitigate ADI

To leverage the strengths of both traditional signal processing and modern deep learning techniques, Zhou et al. [17] proposed a hybrid ADI mitigation system tailored for Quadrature Amplitude Modulation–Orthogonal Frequency Division Multiplexing (QAM-OFDM)-based wireless networks. The architecture of the proposed system is implemented at the receiver side and is composed of seven integrated modules: an analog-to-digital converter, a deep learning-based error compensator, an OFDM demodulator, a deep learning-based interference cancellation unit, a channel equalizer, a forward error correction unit, and a maximum likelihood estimation unit.

The deep learning components of the system incorporate four convolutional neural network (CNN) layers and four Long Short-Term Memory (LSTM) layers. These layers are responsible for capturing spatial and temporal dependencies within the received signal, enabling more precise detection and suppression of ADI-induced distortions. The model was trained using 400 frames and evaluated on 100 test frames. The experimental results demonstrate a significant improvement in communication reliability, with the symbol error rate (SER) being reduced from 0.37618 to 0.0003. This result highlights the potential of hybrid learning-based architectures for real-time and high-accuracy interference mitigation in modern wireless communication environments.

2.4. Other Approaches to Mitigate ADI

Beyond signal processing and learning-based techniques, simulation-driven approaches have also been employed to analyze and evaluate the impact of ADI, particularly in over-the-horizon (OTH) radio communication systems. One such study, conducted by Kai and Wu [18], utilized software simulation to model the propagation characteristics of radio waves within complex atmospheric conditions over non-uniform terrestrial surfaces.

Their analysis was grounded in a detailed digital elevation model (DEM) representing terrain data from Wuxi province to four distinct provinces across China. Key simulation parameters included the transmission frequency, antenna height, elevation angle, polarization mode, propagation angle, and propagation distance. These parameters were meticulously varied to assess their influence on radio wave propagation loss under atmospheric duct conditions.

The simulation results indicated significant signal attenuation across the tested routes, with calculated propagation losses of approximately 150 dB for 100 km links from Wuxi to Hangzhou, Shanghai, and Zhoushan, and a notably higher loss of 237.5 dB on the Wuxi–Nanjing path. These findings underscore the severity of ADI effects in long-distance, low-angle radio transmission scenarios and highlight the utility of simulation tools in pre-deployment analysis and planning for robust network coverage in OTH communication environments.

2.5. Overview of Existing Mitigation Approaches

Several ADI mitigation strategies have been proposed and evaluated across different wireless communication technologies, including TD-LTE and 5G networks. Table 3 provides a comparative overview of representative methodologies, highlighting the diversity in detection mechanisms, performance metrics, and network contexts.

Peralta et al. [10] introduced a Remote Interference Management Reference Signal (RIM-RS) design tailored for 5G NR systems. Their method demonstrated a high detection probability of 0.900 and a remarkably low false alarm probability of 0.002, indicating its reliability and precision in identifying ADI in real-time operational environments.

In another notable study, Zhou et al. [17] presented a hybrid mitigation model combining digital signal processing (DSP), Long Short-Term Memory (LSTM) networks, and convolutional neural networks (CNNs). Applied to QAM-OFDM-based communication systems, their approach achieved a significant improvement in system performance, re-

ducing the symbol error rate from 0.37618 to 0.0003. This result illustrates the efficacy of integrating deep learning with classical signal processing in enhancing ADI mitigation.

Table 3. An overview of the existing mitigation approaches.

Approach	Year	Methodology	Results	Network
Peralta et al. [10]	2019	Remote Interference Management Reference Signal (RIM-RS)	Detection probability: 0.900 False alarm probability: 0.002	5G New Radio (FR1)
Zhou et al. [17]	2020	DSP, LSTM, and CNN	Symbol error rate is reduced from 0.37618 to 0.0003	QAM-OFDM
Zhou et al. [3]	2017	Adjustment of the Guard period	-	TD-LTE
Sun et al. [14]	2017	Adjustment of the Guard period	-	TD-LTE

Zhou et al. [3] proposed an interference mitigation mechanism for TD-LTE networks by adjusting the special subframe configuration, specifically the guard period. While detailed performance metrics were not provided in their study, this approach is recognized for its practical implementation potential within existing LTE infrastructure without requiring significant architectural changes.

Similarly, Sun et al. [14] adopted a guard period adjustment strategy in TD-LTE systems to mitigate ADI. Though this study did not specify quantitative results, it emphasizes system-level configuration tuning as an effective and low-complexity method for interference control.

As summarized in Table 3, these diverse approaches reflect the multidisciplinary nature of ADI mitigation, encompassing signal design, machine learning, hybrid architectures, and protocol-level adjustments. However, variations in evaluation metrics and incomplete performance reporting in some studies underscore the need for standardized benchmarking frameworks to facilitate cross-comparative assessments and advance the field toward more unified, adaptive mitigation solutions.

3. Methodology

This section presents an integrated machine learning (ML) and deep learning (DL) framework for the prediction and mitigation of ADI. The methodology incorporates DSP and ML techniques to characterize ADI behavior and optimize special subframe configurations in TD-LTE systems, with the aim of minimizing interference effects. The experimental setup evaluates the performance and accuracy of the proposed models using real-world TD-LTE network data under practical operating conditions.

Further, ADI ducting heavily depends on the carrier frequency of the radio waves. The degree of interference varies across frequency bands due to their distinct propagation properties. Lower frequencies (e.g., sub-6 GHz) with longer wavelengths diffract and propagate more effectively through atmospheric layers, making them more prone to ducting. Conversely, higher frequencies (e.g., mmWave) with shorter wavelengths experience greater attenuation and are less affected by ducting. At 0.5 GHz, atmospheric ducting is particularly pronounced, as the long wavelength enables radio waves to be trapped in ducts, traveling hundreds of kilometers with minimal loss. This extended range heightens interference risks, as signals from distant transmitters (e.g., base stations) can interfere with receivers far outside their intended range. Therefore, we focused on the low-frequency ranges of the TD-LTE network to develop the ADI mitigation system.

3.1. Atmospheric Duct Interference Prediction

The prediction of ADI strength is critical for proactive interference management in wireless communication networks. ML and DL models have proven effective in forecasting ADI by leveraging both atmospheric and network-side features.

In this study, two prediction approaches were developed and evaluated, differing in the number of features used from the network side while sharing common atmospheric parameters. Both approaches incorporate three key atmospheric features: temperature, pressure, and humidity, which are sourced from the Visual Crossing weather monitoring base station. These features play a crucial role in determining atmospheric refractivity profiles, which directly influence the formation of ducting layers.

The first approach utilizes eight network-side features, whereas the second approach expands this to fifteen network-side features. Common network-side parameters include uplink power values obtained from the operational data of Dialog Axiata PLC, a major mobile network operator in Sri Lanka [7]. The inclusion of a broader feature set in the second approach aims to enhance the model’s sensitivity to subtle interference-related variations across the network.

Both prediction models are trained to classify the strength of ADI into six target classes, which represent different levels of interference severity. The categorization of these classes is detailed in Table 4, serving as a structured framework for evaluating prediction performance and guiding subsequent interference mitigation strategies.

Table 4. The interference range of the target classes.

Target Classes	Min Value	Max Value
Class A	−112.00 dB	
Class B	−116.00 dB	−112.01 dB
Class C	−120.00 dB	−116.01 dB
Class D	−124.00 dB	−120.01 dB
Class E	−128.00 dB	−124.01 dB
Class F		−128.01 dB

This dual-approach design enables comparative analysis of model accuracy and robustness based on feature richness, ultimately contributing to the development of more adaptive and scalable ADI prediction solutions in TD-LTE and 5G environments.

The prediction models are developed in two scenarios. In the first scenario, the features are collected from all ten base stations in the Jaffna district. In the second scenario, the features are collected from only one base station, which is the Jaffna Town base station. The coordinates of the ten base stations in the Jaffna Town district are given in Table 5.

The Support Vector Machine (SVM) model was configured with 11 input features and trained using four different kernel functions—linear, radial basis function (RBF), polynomial, and sigmoid. It employed five-fold cross-validation with a learning rate of 0.001, targeting classification into six ADI severity levels.

Similarly, the Random Forest model was evaluated in two configurations. The first model used 100 estimators, while the second employed 10 estimators with the entropy criterion. Both versions used the same input features and training strategy as the SVM.

The Long Short-Term Memory (LSTM) model was applied in two distinct architectures. In the first approach, it consisted of three layers and was trained for 50 epochs using 11 features. The second approach expanded the feature set to 18 and adopted a four-layer architecture, comprising an input layer (18 neurons), two hidden layers (20 neurons each),

and an output layer (6 neurons). It used the Adam optimizer and mean squared error (MSE) loss, with a learning rate ranging from 0.001 to 0.048.

Table 5. The coordinates of the base stations in the Jaffna district [7].

Base Station	Longitude	Latitude
Palali	80.08	9.79
Karainagar	79.86	9.71
Kandarodai	80.01	9.75
Jaffna	80.00	9.66
Manipai	79.99	9.72
Alaweddy	80.01	9.77
Kankasanthure	80.03	9.81
Nallur	80.03	9.67
Chawakachcheri	80.16	9.65
Kodikamam	80.22	9.68

The convolutional neural network (CNN) was also developed in two approaches. The first model utilized 11 features and consisted of three layers with ReLU activations in the initial two and a SoftMax activation in the final layer. The second CNN model employed 18 features and a four-layer structure, mirroring the configuration of the advanced LSTM model. It used ReLU and SoftMax activations across its layers, along with the Adam optimizer and MSE loss.

In addition, a Stochastic Gradient Descent (SGD) classifier was implemented using 18 features. This model also employed MSE loss and varied the learning rate between 0.001 and 0.048, consistent with the other models. The parameters of the prediction model are given in Table 6.

Table 6. The parameters of the SGD, GB, and XGB classifiers.

Model	SGD Classifier	Gradient Boosting Classifier	Optimized Distributed Gradient Boosting Classifier
Scaler	Standard Scaler	Min-Max Scaler	Min-Max Scaler
Algorithm	SVM: Linear	Random Forest	Random Forest
Dataset shuffled	Yes	Yes	Yes
Estimators	-	100	100
Max-Depth	-	2	2
Max-Features	-	2	2
Loss	MSE	MSE	MSE
Iterations	1000	-	-
Kernel	Linear	-	-
Other features	Macro-average	Macro-average	Macro-average

This study further explored a Gradient Boosting (GB) classifier and an Extreme Gradient Boosting (XGBoost) model. Both utilized 18 features and were trained under the two scenario setups. They were optimized using different learning rates and evaluated using the same classification and validation metrics.

Finally, a cascaded ML-DL hybrid model was constructed to integrate the strengths of both traditional and deep learning techniques. This model’s architecture is illustrated in Figure 1 and detailed in Table 7. It follows the same two-scenario framework and utilizes adaptive learning rates, MSE loss, and a combination of model components for enhanced performance.

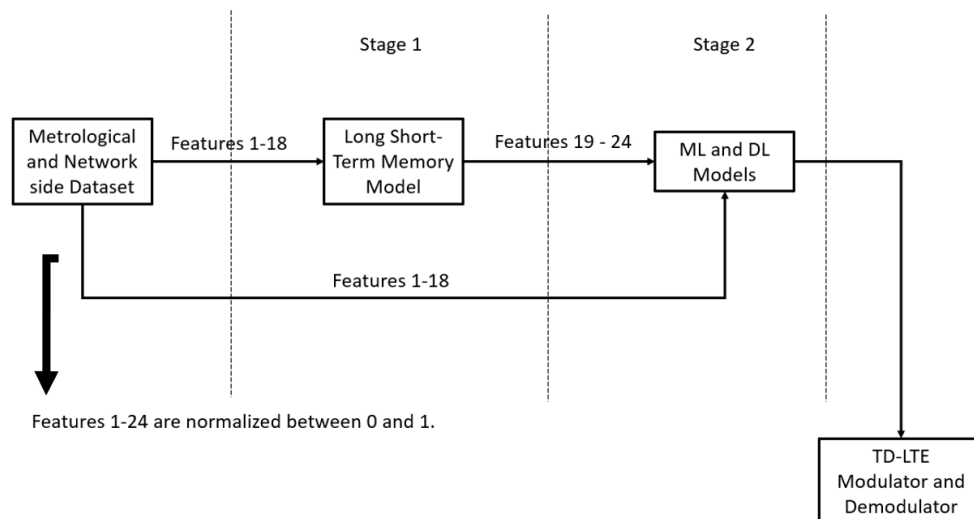


Figure 1. The cascaded ML and DL classifier-based prediction models.

Table 7. The structure of the cascaded prediction models.

Classifiers	Classifier in Stage 1	Classifier in Stage 2
1	LSTM	SDG
2	LSTM	GB
3	LSTM	XGB
4	LSTM	LSTM
5	LSTM	CNN

The dataset contains interference values for the 12 subcarriers of the zeroth physical resource block of the TD-LTE network. Atmospheric duct interference prediction is performed individually in each subcarrier of the physical resource block (i.e., physical resource block 0). One physical resource contains 12 consecutive subcarriers in the TD-LTE systems. The evaluation parameters in the Results and Discussion Section are obtained for the first subcarrier of the zeroth physical resource block. Similarly, we have collected the evaluation parameters for the other subcarriers in the zeroth physical resource block.

3.2. Atmospheric Duct Interference Mitigation

Numerous ADI mitigation systems have been developed over the past decade. However, many of these systems exhibit limitations in terms of mitigation efficiency. These shortcomings highlight a clear research gap in the current state of ADI-related methodologies. To address this gap, a novel ADI mitigation system is proposed. An overview of the proposed framework is illustrated in Figure 2, outlining the key components and operational flow of the system [19,20].

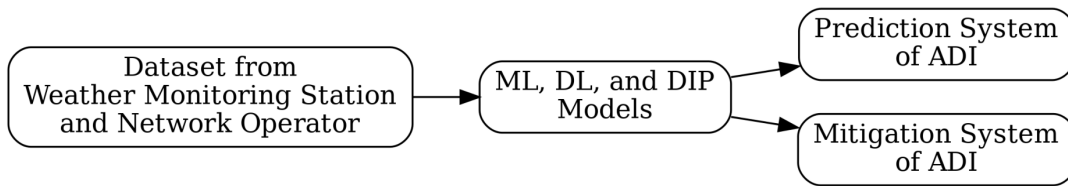


Figure 2. The proposed ADI detection and mitigation system.

In the considered network scenario, there are two groups of base stations: aggressor base stations and victim base stations. The aggressor group comprises six base stations ($m = 6$), while the victim group consists of eight base stations ($n = 8$). This configuration is illustrated in Figure 3. The line-of-sight (LoS) channel, along with the channels affected by atmospheric duct interference (ADI), are associated with the victim base stations, highlighting the impact of interference propagation in the network [21,22].

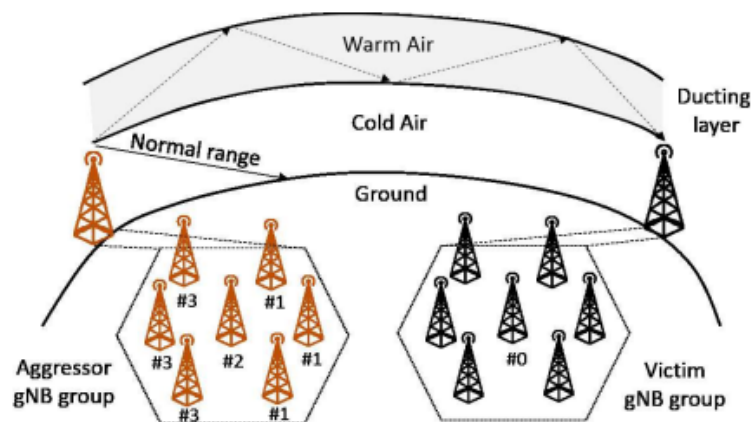


Figure 3. Network setup with six aggressor and eight victim base stations.

One of the key contributions of this research is the adaptive adjustment of the guard period—the time interval between uplink and downlink signals in TD-LTE networks—to mitigate atmospheric duct interference (ADI). By leveraging machine learning models, the system dynamically modifies the guard period in response to detected interference conditions. This approach enables real-time interference management, enhancing the robustness of TD-LTE communications. The structure of the uplink and downlink frames, both with and without atmospheric duct interference, is illustrated in Figure 4 [21,23].

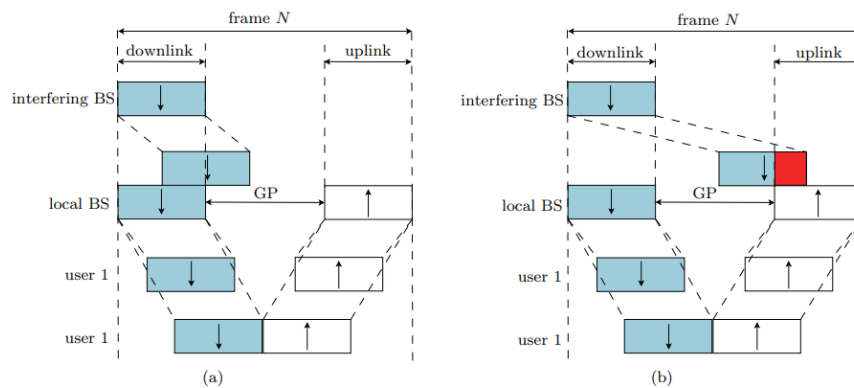


Figure 4. The TD-LTE system (a) without ADI and (b) with ADI [8].

The TD-LTE network uses OFDM to modulate the information-bearing signals in the carrier signal. Figure 5 shows the block diagram of the OFDM modulation and demodulation scheme.

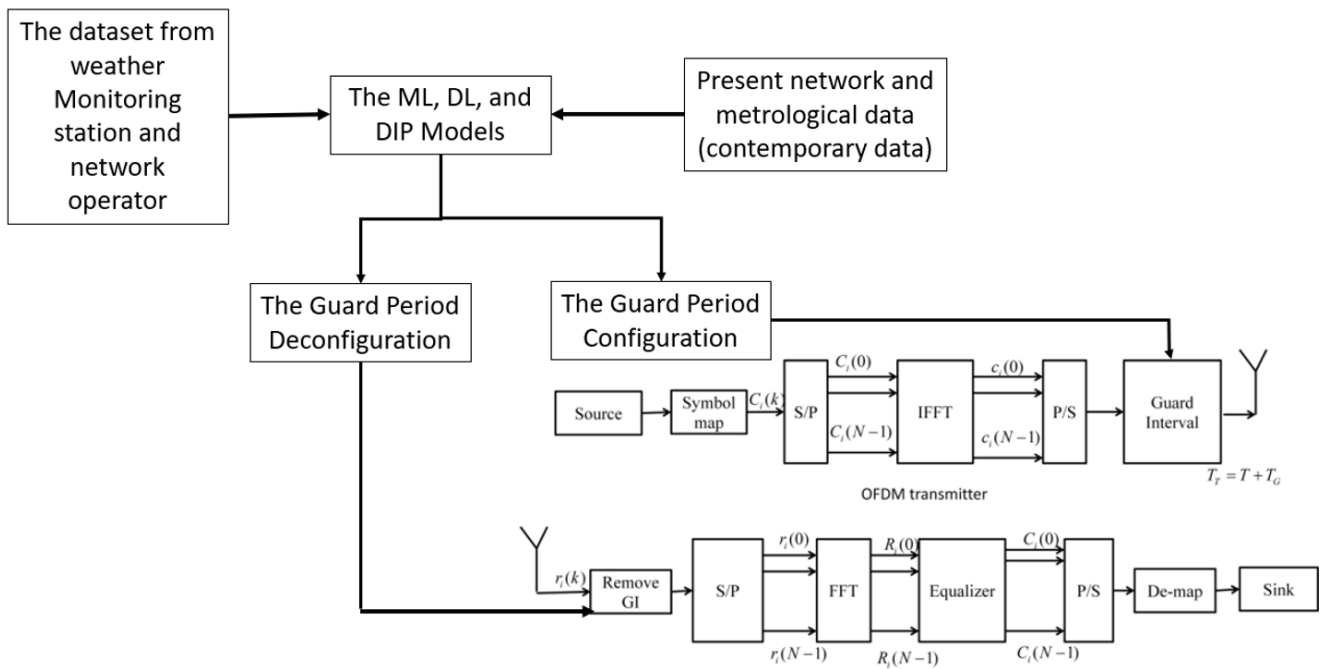


Figure 5. OFDM modulation and demodulation block diagram.

The guard interval between the uplink and downlink signals could be set at the OFDM transmitter block to remove the atmospheric duct interference in the received signal. The guard period configuration could be removed at the OFDM receiver block to identify the transmitted messages. An interference map is created in the data preprocessing stage. The data preprocessing stage is given in Figure 6. This algorithm converts spatial interference measurements into a matrix representation and utilizes Kriging interpolation to estimate unknown values. The method is applied to interference data collected from base stations over a specific district [24,25].

We use three atmospheric side features and fifteen network-side features in the ADI mitigation systems. The three atmospheric side features of the ADI mitigation systems are atmospheric temperature, atmospheric pressure, and atmospheric humidity. The uplink power values of the first frame in the uplinks 0, 1, 2, 3, 4, 5, and 6 and the uplink power values of the last frame in the uplinks 0, 7, 8, 9, 10, 11, 12, and 13 are the fifteen network-side features of the ADI mitigation systems. The features are normalized between 0 and 1 [26,27].

The target of the mitigation system contains six classes. The border values of the target classes are given in Table 8.

Table 8. The border values of the target classes.

Target Classes	Min Value	Max Value
Class A	−112.00 dB	
Class B	−116.00 dB	−112.01 dB
Class C	−120.00 dB	−116.01 dB
Class D	−124.00 dB	−120.01 dB
Class E	−128.00 dB	−124.01 dB
Class F		−128.01 dB

Introduction

The interference level data in the space domain is converted to an $M \times N$ matrix X . The following steps outline the process of generating the interference map using Kriging interpolation.

Definitions:

- lo_i, la_i, le_i : Longitude, latitude, and interference value of the i^{th} measuring point.
- $lo_{\min}, lo_{\max}, la_{\min}, la_{\max}$: Minimum and maximum values of longitude and latitude of the Jaffna district, Sri Lanka.
- le_{\min}, le_{\max} : Minimum and maximum values of the interference level.
- $lo_{\text{step}} = \frac{lo_{\max} - lo_{\min}}{M}$: Longitude step size.
- $la_{\text{step}} = \frac{la_{\max} - la_{\min}}{N}$: Latitude step size.

The matrix $X_{m,n}$ is defined as

$$X_{m,n} = \frac{1}{K} \sum_{i=1}^K le_i \cdot A(lo_i, la_i)$$

where

$$m = 0, 1, 2, \dots, M - 1$$

$$n = 0, 1, 2, \dots, N - 1$$

$$A = [lo_{\min} + m \cdot lo_{\text{step}}, lo_{\min} + (m + 1) \cdot lo_{\text{step}}] \times [la_{\min} + n \cdot la_{\text{step}}, la_{\min} + (n + 1) \cdot la_{\text{step}}]$$

$$A(lo, la) = \begin{cases} 1, & \text{if } lo \in A \text{ and } la \in B \\ 0, & \text{otherwise} \end{cases}$$

Kriging Interpolation

Kriging interpolation is used to estimate unknown points from known points. The estimation of the point (x_0, y_0) is given by

$$Z_0 = \sum_{i=1}^n \lambda_i Z_i$$

where

- Z_0 : Estimated value at (x_0, y_0)
- λ_i : Weight, calculated to minimize $\text{Var}(Z_0 - \bar{Z})$ such that $\mathbb{E}(Z_0 - \bar{Z}) = 0$

Algorithm

- 1: **Input:** The set of longitude, latitude, and interference levels for each base station (BS): lo_i, la_i, le_i
- 2: **Output:** Interference map
- 3: Determine M and N . Usually, $M \times N$ is $\frac{1}{10}$ of the total number of base stations (BS) approximately.
- 4: $X_{m,n} = \frac{1}{K} \sum_{i=1}^K le_i \cdot A(lo_i, la_i)$
- 5: Generate X
- 6: **for** each $x_{i,j} \in X$, if $x_{i,j} = 0$ and (i, j) in the province range **do**
- 7: Use the nearest 30 points of (i, j) to perform Kriging interpolation to get $x_{i,j}$
- 8: **end for**
- 9: **for** each $x_{i,j} \in X$, if $x_{i,j} = 0$ and (i, j) out of the province range **do**
- 10: Set $x_{i,j} = le_{\min}$
- 11: **end for**
- 12: Render X using a heatmap
- 13: **return** Interference map

Figure 6. The data preprocessing algorithm [12,28].

Moreover, a modified formulation of the SNR is employed to better emphasize the influence of interference components within the received signal, as in Equation (1). Under

this formulation, more negative SNR values indicate a higher signal power relative to interference (noise). This approach enables the model to effectively prioritize and monitor scenarios with pronounced interference characteristics, which are particularly important in ADI conditions in TD-LTE networks.

$$SNR = -10\log_{10} \frac{Signal\ Power}{Noise\ Power} \tag{1}$$

The mitigation models were also developed under two distinct scenarios. In Scenario One, feature data were collected from all ten base stations located within the Jaffna district. In Scenario Two, data were obtained exclusively from a single base station—specifically, the Jaffna Town base station. The geographical coordinates of all ten base stations in the Jaffna district are provided in Table 5.

Further, there are three special subframes in TD-LTE communication frames: the uplink pilot time slot (UPPTS), the downlink pilot time slot (DWPTS), and the guard period (GP). These special subframes can be dynamically configured or de-configured based on the decisions made by the ADI mitigation models. The specific configuration of these subframes within the ADI mitigation system is presented in Table 9 [29].

Table 9. The configuration of the special subframes.

Config. ID	Conventional Configuration Approach			Extended Configuration Approach		
	DWPTS	GP	UPPTS	DWPTS	GP	UPPTS
C1	3	10	1	3	8	1
C2	3	9	2	3	7	2
C3	9	4	1	8	3	1
C4	8	4	2	8	2	2
C5	10	3	1	9	2	1
C6	10	2	2	9	1	2
C7	12	1	1	10	1	1
C8	11	1	2	8	2	2

As in the case of the prediction models, the dataset contains interference values for the 12 subcarriers of the zeroth physical resource block (PRB) in the TD-LTE network. Atmospheric duct interference (ADI) mitigation is performed individually on each subcarrier within this PRB. In TD-LTE systems, a single PRB comprises 12 consecutive subcarriers. The evaluation parameters presented in the Results and Discussion Section are derived from the first subcarrier of the zeroth PRB. The reported Signal-to-Noise Ratio (SNR) and Bit Error Rate (BER) values correspond to the model outputs for this specific subcarrier. Both the SNR and BER are measured using the Remcom wireless Insite MIMO version (2022 release).

Next, various classifiers, including the GB classifier, LSTM classifier, CNN classifier, ODGB classifier, SGD classifier, and Histogram-based Gradient Boosting (HGB) classifier, were investigated for ADI mitigation. Each classifier was tested using three distinct models with varying hyperparameters, as illustrated in Figure 7, where x represents the classifier ($x \in \{1, 2, 3, 4, 5, 6\}$) and y denotes the models with different hyperparameters ($y \in \{1, 2, 3\}$).

Furthermore, for each classifier, the models with different hyperparameters were combined using ensemble learning to identify the best-performing classifier for ADI mitigation. In this approach, Model Y_a and Y_b of Classifier x are ensembled, and their combined feature output is passed through Model Y_a of Classifier x in a second stage. This final stage is used to configure the guard period for interference mitigation, as shown in Figure 8.

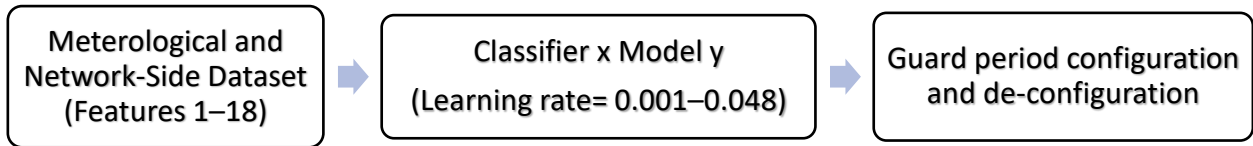


Figure 7. Block diagram of Model Y within Classifier X, designed for ADI mitigation in the proposed system.



Figure 8. Block diagram of the ensemble-based ADI mitigation system, illustrating the integration of Classifier X with sub-models Y_a and Y_b to enhance detection accuracy and robustness against atmospheric duct interference.

We transmitted 53 random symbols in the mitigation system and observed the Bit Error Rate and the Signal-to-Noise Ratio at the receiver side of the mitigation system. Also, the Signal-to-Noise Ratios of the ADI mitigation systems with different learning rates are measured at the receiver side.

The hyperparameter configurations of the three models for each classifier—GB, LSTM, CNN, ODGB, SGD, and HGB—are presented in Table 10, Table 11, Table 12, Table 13, Table 14, and Table 15, respectively.

Table 10. The parameters of the three different GB models.

Parameters	Model 1	Model 2	Model 3
Scaler	Min-Max Scaler	Min-Max Scaler	Min-Max Scaler
Dataset shuffled	Yes	Yes	Yes
Estimators	125	135	145
Criterion	Friedman MSE	Squared Error	Friedman MSE
Max-Depth	3	4	5
Max-Features	4	5	3
Loss	Log loss	Log loss	Log loss
Minimum sample leaf	4	3	5
Minimum sample split	3	5	3
Minimum weight fraction leaf	0.10	0.15	0.20
Maximum depth	2	3	4
Average	Macro-average	Macro-average	Macro-average
Learning rate	0.001–0.048	0.001–0.048	0.001–0.048

Table 11. The parameters of the three different LSTM models.

Parameters	LSTM Model 1	LSTM Model 2	LSTM Model 3
Dataset	Time series	Time series	Time series
Encoder	Label encoder	Label encoder	Label encoder
Optimizer	Adam	Adam	Adam
Loss	Log loss	Log loss	Log loss
Activation	Tanh	ReLu	ReLu
Recurrent activation	Sigmoid	Sigmoid	Tanh
Dropout	0.10	0.15	0.20
Recurrent dropout	0.20	0.10	0.15
Input layer	18 neurons	18 neurons	18 neurons
Hidden layer 1–3	20 neurons	22 neurons	24 neurons
Hidden layer 4–6	22 neurons	24 neurons	20 neurons
Output layer	6 neurons	6 neurons	6 neurons
Learning rate	0.001–0.048	0.001–0.048	0.001–0.048

Table 12. The parameters of the three different CNN models.

Parameters	CNN Model 1	CNN Model 2	CNN Model 3
Dataset	Shuffled	Shuffled	Shuffled
Encoder	One Hot encoder	One Hot encoder	One Hot encoder
Optimizer	Adam	Adam	Adam
Loss	Log loss	Log loss	Log loss
Input layer	18 neurons, ReLu	18 neurons, ReLu	18 neurons, Tanh
Hidden layer 1	18 neurons, ReLu	20 neurons, ReLu	20 neurons, Tanh
Hidden layer 2	20 neurons, Sigmoid	22 neurons, Tanh	24 neurons, Sigmoid
Hidden layer 3	18 neurons, ReLu	20 neurons, ReLu	20 neurons, Tanh
Hidden layer 4	20 neurons, Sigmoid	22 neurons, Tanh	24 neurons, Sigmoid
Hidden layer 5	18 neurons, ReLu	20 neurons, ReLu	20 neurons, Tanh
Hidden layer 6	20 neurons, Sigmoid	22 neurons, Tanh	24 neurons, Sigmoid
Output layer	6 neurons, Sigmoid	6 neurons, Tanh	6 neurons, Tanh
Learning rate	0.001–0.048	0.001–0.048	0.001–0.048

Table 13. The parameters of the three different ODGB models.

Parameters	ODGB Model 1	ODGB Model 2	ODGB Model 3
Scaler	Min-Max Scaler	Min-Max Scaler	Min-Max Scaler
Dataset shuffled	Yes	Yes	Yes
Gamma	2	4	4
Max depth	4	3	3
Minimum child weight	2	3	4
Max delta step	3	4	3
Sampling method	Uniform	Gradient-based	Uniform
Lamda	2	3	4
Tree method	Auto	Exact	Auto
Process type	Default	Update	Default
Max bin	128	128	256
Average	Macro-average	Macro-average	Macro-average
Learning rate	0.001–0.048	0.001–0.048	0.001–0.048

Table 14. The parameters of the three different SGD models.

Parameters	SGD Model 1	SGD Model 2	SGD Model 3
Scaler	Standard Scaler	Standard Scaler	Standard Scaler
Dataset shuffled	Yes	Yes	Yes
Validation fraction	0.03	0.04	0.02
Verbose	0.02	0.03	0.04
Tolerance	0.002	0.001	0.003
Fit Intercept	True	False	True
Alpha	0.004	0.002	0.003
Penalty	L2	L1	L2
Loss	Log loss	Log loss	Log loss
Maximum iterations	900	800	750
Kernel	Linear	Linear	Linear
Average	Macro-average	Macro-average	Macro-average
Learning rate	0.001–0.048	0.001–0.048	0.001–0.048

Table 15. The parameters of the three different HGB models.

Parameters	HGB Classifier 1	HGB Classifier 2	HGB Classifier 3
Scaler	Min-Max Scaler	Min-Max Scaler	Min-Max Scaler
Dataset shuffled	Yes	Yes	Yes
Loss	Log loss	Log loss	Log loss
Maximum iteration	125	150	175
Maximum leaf nodes	20	25	30
Minimum sample leaf	10	15	20
L2 regularization	0.2	0.15	0.25
Maximum bins	127	255	127
Early stopping	Auto	Bool	Auto
Validation fraction	0.2	0.15	0.15
Tolerance	0.001	0.002	0.0025
Average	Macro-average	Macro-average	Macro-average
Learning rate	0.001–0.048	0.001–0.048	0.001–0.048

4. Results and Discussion

4.1. The Results of the ADI Prediction Models

As elaborated in Section 3, the prediction models are developed under two scenarios to evaluate their generalizability and adaptability under varying data conditions. In Scenario One, features are collected from all ten base stations in the Jaffna district, providing a diverse and comprehensive dataset that captures a wide range of network behaviors and atmospheric conditions. This setup is aimed at building models capable of recognizing generalized patterns across a broader geographic area. In contrast, Scenario Two focuses on a localized dataset, using features from only a single base station—Jaffna Town—to assess the model’s performance in a constrained, site-specific environment. This comparison helps determine whether accurate predictions can still be achieved with limited, location-specific data, which is often the case in real-world deployments.

4.1.1. The Evaluation Parameters of the ML- and DL-Based ADI Models

The evaluation parameters of the SVM-, RF-, LSTM-, and CNN-based ADI prediction models are given in Table 16. The model uses a 5-fold cross-validation approach. The learning rate is maintained at 0.001. The evaluation parameters are measured in two scenarios,

which are the training dataset and the test dataset. Also, the evaluation parameters are compared with the literature.

Table 16. The evaluation parameters of the ML and DL models, with a comparison of the state of the art.

	Accuracy		Precision		Recall		F1 Score	
	Train	Test	Train	Test	Train	Test	Train	Test
ML models								
KNN [8]	-	0.670	-	-	-	-	-	-
SVM [8]	-	0.650	-	-	-	-	-	-
SVM linear	0.635	0.634	0.390	0.387	0.355	0.355	0.302	0.301
SVM rbf	0.686	0.672	0.665	0.623	0.485	0.463	0.508	0.478
SVM polynomial	0.677	0.668	0.706	0.682	0.467	0.451	0.487	0.465
SVM sigmoid	0.524	0.522	0.302	0.301	0.302	0.301	0.278	0.278
Random forest [13]	-	0.650	-	-	-	-	-	-
Random forest M1	0.999	0.723	0.999	0.657	0.999	0.573	0.999	0.594
Random forest M2	0.999	0.721	0.999	0.636	0.999	0.566	0.999	0.593
LSTM [26]	-	0.984	-	-	-	-	-	-
LSTM	0.636	0.574	0.477	0.413	0.432	0.443	0.412	0.342
CNN [15]	-	0.856	-	-	-	-	-	-
CNN [17]	0.990	0.977	-	-	-	-	-	-
CNN	0.655	0.653	0.562	0.562	0.456	0.450	0.464	0.455

Among the models tested, convolutional neural networks (CNNs) demonstrated strong generalization capabilities, with the CNN [17] achieving the highest test accuracy (0.977), though detailed performance metrics were not provided. Random Forest models (M1 and M2) achieved excellent F1 scores near 0.59. Support Vector Machines (SVMs) with radial basis function (RBF) and polynomial kernels performed well, showing a good balance between accuracy and generalization. In contrast, linear and sigmoid SVMs performed poorly across all metrics. Long Short-Term Memory (LSTM) models showed moderate performance, with relatively low F1 scores, indicating challenges in precision and recall despite their ability to handle sequential data. Overall, CNNs and Random Forests emerged as the most effective models, with SVMs offering a balanced alternative, while LSTM and sigmoid-based approaches were less suitable without further optimization.

4.1.2. The Evaluation Parameters of the ML and DL Classifier-Based Prediction Model

The evaluation parameters of the ML and DL classifier-based prediction models are given in Table 17. The results are given for both Scenario One and Scenario Two.

The evaluation results of the machine learning (ML) and deep learning (DL) classifier-based models under both scenarios reveal key insights into their predictive performance for atmospheric duct interference. In Scenario One, where data are collected from all ten base stations, the Gradient Boosting Classifier (GBC) and Optimized Distributed Gradient Boosting (XGB) models achieved the highest test accuracy of 0.77, with XGB showing better overall balance across precision (0.79), recall (0.61), and F1 score (0.63), along with a relatively low mean squared error (MSE) of 0.26. The CNN classifier also performed well, achieving a test accuracy of 0.75 and the lowest MSE of 0.11, although its F1 score (0.30) was comparatively lower.

In Scenario Two, which uses data from a single base station, the Stochastic Gradient Descent (SGD) model showed the most improvement, increasing its test accuracy to 0.85, precision to 0.79, and F1 score to 0.74, with an MSE of 0.25. The CNN classifier again demonstrated strong performance, matching its Scenario One accuracy (0.77), while achiev-

ing the highest precision (0.83) and recall (0.77) across all models in this scenario and the lowest MSE of 0.09.

Table 17. The evaluation parameters of the ML and DL classifier-based prediction models.

Classifier	Scenario One						Scenario Two					
	Learning Rate	Test Accuracy	Test Precision	Test Recall	Test F1 Score	MSE Loss	Learning Rate	Test Accuracy	Test Precision	Test Recall	Test F1 Score	MSE Loss
Stochastic gradient descent	0.024	0.68	0.55	0.65	0.58	0.36	0.012	0.85	0.79	0.70	0.74	0.25
Gradient boosting classifier	0.048	0.77	0.75	0.55	0.58	0.32	0.048	0.72	0.60	0.55	0.55	0.32
Optimized distributed gradient boosting classifier	0.008	0.77	0.79	0.61	0.63	0.26	0.012	0.72	0.62	0.58	0.58	0.34
Long short-term memory classifier	0.001	0.70	0.71	0.69	0.20	0.14	0.012	0.66	0.70	0.60	0.40	0.15
Convolutional neural network classifier	0.024	0.75	0.78	0.75	0.30	0.11	0.016	0.77	0.83	0.77	0.40	0.09

Overall, CNN and Gradient Boosting-based models consistently showed robust performance in both scenarios, while the SGD classifier significantly improved with localized data. These results suggest that model effectiveness varies with data granularity, and that CNN classifiers in particular offer high precision and efficiency even with limited input data.

4.1.3. The Evaluation Parameters of the Cascaded ML and DL Classifier-Based Prediction Model

The evaluation parameters of the cascaded ML and DL classifier-based prediction models are given in Table 18. The results are given for both Scenarios One and Scenario Two. The performance of the cascaded machine learning (ML) and deep learning (DL) classifier-based prediction models across two scenarios reveals a nuanced variation in accuracy, precision, and other evaluation metrics. In Scenario One, Classifier 2 achieved the highest accuracy at 0.69, alongside a precision of 0.60 and an F1 score of 0.54. Although Classifier 5 and the LSTM model showed comparable accuracy values (0.68 and 0.70, respectively), their F1 scores were significantly lower at 0.20, indicating a reduced balance between precision and recall. Most classifiers demonstrated moderate precision and recall, with MSE values ranging between 0.14 and 0.45, suggesting room for optimization in model generalization.

Table 18. The evaluation parameters of the ML and DL cascaded -based prediction models.

Classifier	Scenario One						Scenario Two					
	Learning Rate	Test Accuracy	Test Precision	Test Recall	Test F1 Score	MSE Loss	Learning Rate	Test Accuracy	Test Precision	Test Recall	Test F1 Score	MSE Loss
LSTM	0.001	0.70	0.71	0.69	0.20	-	0.012	0.66	0.70	0.60	0.40	-
Classifier 1	0.024	0.66	0.55	0.62	0.55	0.43	0.024	0.70	0.62	0.64	0.60	0.37
Classifier 2	0.048	0.69	0.60	0.52	0.54	0.42	0.048	0.72	0.75	0.64	0.63	0.34
Classifier 3	0.020	0.67	0.59	0.53	0.48	0.45	0.028	0.70	0.70	0.59	0.57	0.40
Classifier 4	0.001	0.62	0.64	0.55	0.10	0.16	0.001	0.63	0.66	0.60	0.05	0.16
Classifier 5	0.008	0.68	0.70	0.63	0.20	0.14	0.008	0.67	0.70	0.62	0.20	0.14

In Scenario Two, the overall model performance generally improved. Classifier 2 once again stood out, increasing its test accuracy to 0.72 and achieving the highest precision (0.75) and a solid F1 score of 0.63, coupled with a relatively low MSE of 0.34. Classifier 1 and Classifier 3 also saw improvements in both accuracy and F1 scores, while LSTM showed a slight drop in accuracy to 0.66 but a marked increase in its F1 score to 0.40, indicating better precision–recall trade-off under localized data. Notably, Classifiers 4 and 5 maintained low F1 scores (0.05 and 0.20, respectively), despite consistent precision values, suggesting challenges in achieving effective recall.

Overall, the results demonstrate that the cascaded models benefit from scenario-specific tuning, with classifiers like Classifier 2 showing strong adaptability. Localized training data, as in Scenario Two, appears to support better predictive consistency for several models.

4.2. The Results of the ADI Mitigation Models

4.2.1. The Results of the GB Classifier-Based ADI Mitigation System

The evaluation parameters of the GB classifier-based ADI mitigation models are given in Table 19. The results are given for both scenarios one and two. The BER and SNR of the GB-based ADI mitigation systems were evaluated at the receiver side for different learning rates. The results are presented in Table 20.

Table 19. The evaluation parameters of the GB classifier-based ADI mitigation models.

Classifier	Scenario One						Scenarios Two					
	Learning Rate	Test Accuracy	Test Precision	Test Recall	Test F1 Score	Log Loss	Learning Rate	Test Accuracy	Test Precision	Test Recall	Test F1 Score	Log Loss
GB Model 1	0.004	0.67	0.68	0.52	0.52	0.24	0.012	0.62	0.66	0.57	0.56	0.19
GB Model 2	0.012	0.68	0.75	0.68	0.36	0.12	0.024	0.61	0.60	0.57	0.58	0.10
GB Model 3	0.008	0.67	0.68	0.53	0.55	0.19	0.024	0.62	0.65	0.60	0.41	0.14
GB Model 1 and 2	0.028	0.67	0.67	0.68	0.42	0.14	0.012	0.60	0.62	0.54	0.39	0.18
GB Model 2 and 3	0.012	0.68	0.72	0.56	0.55	0.19	0.016	0.61	0.61	0.59	0.56	0.13

Table 20. The Bit Error Rates of the GB classifier-based mitigation systems with different learning rates.

Classifier	BER						SNR					
	Learning Rate	Conventional Configuration Approach		Extended Configuration Approach		Learning Rate	Conventional Configuration Approach (dB)		Extended Configuration Approach (dB)			
GB	Dataset Is Collected from All the 10 Base Stations	Dataset Is Collected from Only One Base Station	Dataset Is Collected from All the 10 Base Stations	Dataset Is Collected from All the 10 Base Stations	Dataset Is Collected from Only One Base Station	Dataset Is Collected from All the 10 Base Stations	Dataset Is Collected from Only One Base Station	Dataset Is Collected from All the 10 Base Stations	Dataset Is Collected from Only One Base Station	Dataset Is Collected from Only One Base Station	Dataset Is Collected from All the 10 Base Stations	Dataset Is Collected from Only One Base Station
Model 1	0.004	0.012	0.003	0.002	0.004	0.003	0.004	0.012	−11.40	−10.30	−11.30	−10.10
Model 2	0.012	0.024	0.002	0.003	0.002	0.002	0.012	0.024	−09.20	−09.30	−10.20	−10.30
Model 3	0.008	0.024	0.004	0.003	0.003	0.004	0.008	0.024	−11.30	−13.40	−12.40	−13.50
Model 1 and 2	0.028	0.012	0.002	0.002	0.003	0.003	0.028	0.012	−10.20	−10.30	−10.40	−09.60
Model 2 and 3	0.012	0.016	0.002	0.003	0.003	0.002	0.012	0.016	−10.20	−10.40	−09.80	−10.40

In Table 19, individual models (Model 1, 2, and 3) and model ensembles (Model 1 and 2, and Model 2 and 3) were tested. In Scenario One (data from all base stations), Model 2 achieved the highest precision (0.75) and F1 score (0.36), indicating better mitigation effectiveness, while Model 1 and Model 2 had the best recall (0.68). In Scenario Two (data from a single base station), Model 3 performed slightly better in F1 score (0.41), showing its adaptability to more localized conditions.

Table 20 presents the BER and SNR for both conventional and extended configuration approaches across different learning rates. The extended configuration consistently yielded lower BER and higher SNR, indicating better signal quality and error resilience. For instance, Model 3 with a 0.024 learning rate showed the lowest BER (0.002–0.003) and the highest SNR (up to −13.5 dB). This suggests that model ensembling and configuration extension enhance ADI mitigation performance, especially under the varied channel conditions represented in the two scenarios.

4.2.2. The Results of the LSTM Classifier-Based ADI Mitigation System

The performance metrics of the LSTM classifier-based ADI mitigation models for both Scenario One and Scenario Two are summarized in Table 21. Additionally, Table 22 presents the BER and SNR values of the LSTM-based mitigation systems, measured at the receiver side across various learning rates.

Table 21. The evaluation parameters of the LSTM classifier-based ADI mitigation models.

Classifier	Scenario One						Scenario Two					
	Learning Rate	Test Accuracy	Test Precision	Test Recall	Test F1 Score	Log Loss	Learning Rate	Test Accuracy	Test Precision	Test Recall	Test F1 Score	Log Loss
LSTM												
Model 1	0.012	0.62	0.67	0.62	0.55	0.24	0.024	0.62	0.61	0.63	0.48	0.16
Model 2	0.004	0.61	0.69	0.66	0.48	0.21	0.024	0.62	0.68	0.53	0.38	0.24
Model 3	0.008	0.63	0.74	0.58	0.45	0.11	0.016	0.64	0.67	0.62	0.47	0.15
Model 1 and 2	0.012	0.62	0.60	0.61	0.33	0.11	0.016	0.65	0.70	0.66	0.49	0.23
Model 2 and 3	0.028	0.68	0.62	0.68	0.50	0.10	0.012	0.65	0.67	0.61	0.39	0.13

Table 22. The Bit Error Rates of the LSTM classifier-based mitigation systems with different learning rates.

Classifier	Learning Rate	BER				SNR						
		Conventional Configuration Approach		Extended Configuration Approach		Conventional Configuration Approach (dB)		Extended Configuration Approach (dB)				
LSTM												
Model 1	0.012	Dataset Is Collected from All the 10 Base Stations	Dataset Is Collected from Only One Base Station	Dataset Is Collected from All the 10 Base Stations	Dataset Is Collected from Only One Base Station	Dataset Is Collected from All the 10 Base Stations	Dataset Is Collected from Only One Base Station	Dataset Is Collected from All the 10 Base Stations	Dataset Is Collected from Only One Base Station	Dataset Is Collected from All the 10 Base Stations	Dataset Is Collected from Only One Base Station	
Model 2	0.004	0.024	0.002	0.004	0.003	0.004	0.012	0.024	−09.10	−10.40	−10.20	−12.20
Model 3	0.008	0.016	0.005	0.002	0.004	0.002	0.008	0.016	−11.30	−11.40	−11.20	−11.30
Model 1 and 2	0.012	0.016	0.002	0.003	0.003	0.003	0.012	0.016	−10.10	−10.90	−10.30	−10.80
Model 2 and 3	0.028	0.012	0.002	0.003	0.003	0.002	0.028	0.012	−10.30	−10.10	−11.10	−10.30

The performance evaluation of the LSTM-based ADI mitigation system reveals consistent results across both test scenarios. In terms of classification metrics, Model 3 exhibited substantial precision in both scenarios, with a notably low log loss, suggesting confident and accurate predictions. Among all combinations, the Model 2 and Model 3 ensemble achieved the highest accuracy (0.68) in Scenario One and maintained solid recall and F1 scores, making it a strong candidate for effective ADI detection and mitigation. Scenario Two showed slightly better overall balance in precision and recall across different models, especially for the Model 1 and 2 ensemble.

The BER and SNR analysis in Table 22 supports the classification performance. The extended configuration approach consistently outperformed the conventional method, showing lower BER values and higher SNR values across most models and learning rates. Notably, Model 2 and Model 3 maintained low BER and high SNR, especially when data were sourced from all ten base stations, underscoring their robustness in diverse deployment conditions. Overall, the results indicate that LSTM classifiers—especially when ensembled—are highly effective in mitigating ADI under varying learning rates and data sources.

4.2.3. The Results of the CNN Classifier-Based ADI Mitigation System

The performance metrics for the CNN-based ADI mitigation models under both Scenario One and Scenario Two are summarized in Table 23. Additionally, the Bit Error Rate (BER) and Signal-to-Noise Ratio (SNR) for the CNN-based mitigation systems, evaluated at the receiver side for various learning rates, are presented in Table 24.

Table 23. The evaluation parameters of the CNN classifier-based ADI mitigation models.

Classifier	Scenario One						Scenarios Two					
	Learning Rate	Test Accuracy	Test Precision	Test Recall	Test F1 Score	Log Loss	Learning Rate	Test Accuracy	Test Precision	Test Recall	Test F1 Score	Log Loss
CNN Model 1	0.012	0.61	0.74	0.64	0.37	0.15	0.004	0.67	0.72	0.54	0.45	0.14
Model 2	0.016	0.64	0.75	0.53	0.50	0.20	0.024	0.63	0.67	0.62	0.47	0.21
Model 3	0.004	0.66	0.63	0.64	0.34	0.21	0.028	0.61	0.61	0.64	0.53	0.21
Model 1 and 2	0.016	0.60	0.69	0.65	0.52	0.22	0.016	0.61	0.69	0.61	0.42	0.19
Model 2 and 3	0.028	0.61	0.66	0.56	0.56	0.12	0.008	0.60	0.64	0.53	0.43	0.24

The evaluation of the CNN classifier-based ADI mitigation system reveals varying levels of performance across different models and scenarios. In Scenario One, the highest test accuracy (0.66) was achieved by Model 3 at a learning rate of 0.004, though it had a relatively low F1 score (0.34). Model 2 showed a balanced performance with a test accuracy of 0.64 and a higher F1 score of 0.50, suggesting a more reliable balance between precision and recall. The combination of Model 2 and 3 offered slightly improved F1 performance (0.56) with decent precision and recall, indicating its effectiveness in mitigating ADI while maintaining model robustness. In Scenario Two, Model 1 outperformed others in terms of test accuracy (0.67) and had a moderate F1 score (0.45), while the highest F1 score (0.53) was achieved by Model 3. The model combination strategies in this scenario did not significantly enhance performance metrics over individual models.

In terms of the Bit Error Rate (BER) and Signal-to-Noise Ratio (SNR), as shown in Table 24, the CNN-based mitigation systems consistently showed better performance under the extended configuration approach, especially when datasets from multiple base stations were used. Model 3 achieved the lowest BER (0.003) and highest SNR values (−13.70 dB

and -13.20 dB) under these conditions, highlighting its strong capability in reducing interference effects. Similarly, Model 2 also performed well with a low BER and a high SNR under the extended setup, particularly with a learning rate of 0.016.

Table 24. The Bit Error Rates of the CNN classifier-based mitigation systems with different learning rates.

Classifier	BER						SNR					
	Learning Rate		Conventional Configuration Approach		Extended Configuration Approach		Learning Rate		Conventional Configuration Approach (dB)		Extended Configuration Approach (dB)	
	Dataset Is Collected from All the 10 Base Stations	Dataset Is Collected from Only One Base Station	Dataset Is Collected from All the 10 Base Stations	Dataset Is Collected from All the 10 Base Stations	Dataset Is Collected from Only One Base Station	Dataset Is Collected from All the 10 Base Stations	Dataset Is Collected from Only One Base Station	Dataset Is Collected from All the 10 Base Stations	Dataset Is Collected from Only One Base Station	Dataset Is Collected from Only One Base Station	Dataset Is Collected from All the 10 Base Stations	Dataset Is Collected from Only One Base Station
Model 1	0.012	0.004	0.002	0.004	0.003	0.003	0.012	0.004	-10.20	-11.90	-10.40	-12.40
Model 2	0.016	0.024	0.003	0.005	0.004	0.005	0.016	0.024	-11.20	-12.40	-11.20	-13.80
Model 3	0.004	0.028	0.005	0.004	0.005	0.003	0.004	0.028	-13.20	-11.40	-13.70	-11.80
Model 1 and 2	0.016	0.016	0.002	0.003	0.003	0.003	0.016	0.016	-10.30	-10.30	-11.20	-11.50
Model 2 and 3	0.028	0.008	0.004	0.004	0.004	0.004	0.028	0.008	-12.40	-11.40	-13.40	-12.50

4.2.4. The Results of the ODGB Classifier-Based ADI Mitigation System

Table 25 outlines the performance metrics of the ODGB classifier models developed for ADI mitigation under both Scenario One and Scenario Two. In addition to classification accuracy and related parameters, the impact of varying learning rates on system performance was examined. Correspondingly, Table 26 presents the Bit Error Rate (BER) and Signal-to-Noise Ratio (SNR) measurements obtained at the receiver end, offering further insights into the effectiveness of ODGB-based mitigation strategies.

Table 25. The evaluation parameters of the ODGB classifier-based ADI mitigation models.

Classifier	Scenario One						Scenarios Two					
	Learning Rate	Test Accuracy	Test Precision	Test Recall	Test F1 Score	Log Loss	Learning Rate	Test Accuracy	Test Precision	Test Recall	Test F1 Score	Log Loss
Model 1	0.004	0.68	0.65	0.56	0.55	0.23	0.012	0.68	0.66	0.55	0.46	0.25
Model 2	0.008	0.64	0.63	0.62	0.35	0.22	0.016	0.66	0.62	0.70	0.54	0.22
Model 3	0.012	0.66	0.62	0.67	0.53	0.21	0.008	0.64	0.62	0.54	0.31	0.18
Model 1 and 2	0.016	0.63	0.65	0.62	0.34	0.24	0.012	0.61	0.62	0.61	0.32	0.25
Model 2 and 3	0.016	0.66	0.73	0.63	0.44	0.19	0.028	0.63	0.67	0.61	0.33	0.22

In Table 25, the classification accuracy, precision, recall, F1 score, and log loss of the models are compared under two scenarios. Scenario One shows that Model 1 achieves a classification accuracy of 0.68 with a learning rate of 0.004, and in Scenario Two, Model 1 maintains the same accuracy with a learning rate of 0.012. Precision values remain between 0.65 and 0.66 across models, indicating a moderate ability to correctly identify positive instances. Recall varies more significantly, with Model 1 in Scenario One having a recall of 0.56, while other models, like Model 2 in Scenario Two, achieve a recall of 0.62, indicating a better identification of positive instances. The F1 scores, which balance precision and recall,

range from 0.55 to 0.70, with some models exhibiting better overall balance. Log loss values vary between 0.18 and 0.25, suggesting a moderate degree of accuracy in prediction, with minimal fluctuation across different learning rates and models.

Table 26. The Bit Error Rates of the ODGB classifier-based mitigation systems with different learning rates.

Classifier	BER						SNR					
	Learning Rate		Conventional Configuration Approach		Extended Configuration Approach		Learning Rate		Conventional Configuration Approach (dB)		Extended Configuration Approach (dB)	
	Dataset Is Collected from All the 10 Base Stations	Dataset Is Collected from Only One Base Station	Dataset Is Collected from All the 10 Base Stations	Dataset Is Collected from All the 10 Base Stations	Dataset Is Collected from Only One Base Station	Dataset Is Collected from All the 10 Base Stations	Dataset Is Collected from Only One Base Station	Dataset Is Collected from All the 10 Base Stations	Dataset Is Collected from Only One Base Station	Dataset Is Collected from Only One Base Station	Dataset Is Collected from All the 10 Base Stations	Dataset Is Collected from Only One Base Station
Model 1	0.004	0.012	0.005	0.004	0.005	0.004	0.004	0.012	−13.90	−12.80	−13.50	−11.80
Model 2	0.008	0.016	0.003	0.004	0.004	0.003	0.008	0.016	−12.60	−12.30	−11.90	−11.90
Model 3	0.012	0.008	0.005	0.004	0.004	0.004	0.012	0.008	−13.30	−13.40	−13.70	−12.90
Model 1 and 2	0.016	0.012	0.002	0.005	0.002	0.005	0.016	0.012	−11.30	−14.20	−11.40	−14.10
Model 2 and 3	0.016	0.028	-	-	-	-	0.016	0.028	-	-	-	-

In Table 26, the Bit Error Rate (BER) and Signal-to-Noise Ratio (SNR) are examined at different learning rates for both conventional and extended configuration approaches. The BER shows a general decrease as the learning rate increases, which indicates better performance in terms of error reduction with higher learning rates. For example, in Model 1, the BER is lower when using a dataset collected from all ten base stations compared to just one base station. The SNR also improves with higher learning rates, particularly in the extended configuration. For instance, in Model 1, the SNR values range from −13.90 dB to −11.80 dB as the learning rate increases, showing improved signal quality under extended configurations.

Overall, the results suggest that the ODGB-based mitigation system benefits from higher learning rates, leading to improved accuracy, reduced error rates (BER), and better signal clarity (SNR). However, the performance improvements are moderate and vary across different models and configurations, highlighting the need for further optimization and fine-tuning of learning rates for enhanced system performance.

4.2.5. The Results of the SGD Classifier-Based ADI Mitigation System

The evaluation parameters of the SGD classifier-based ADI mitigation models are given in Table 27. The results are given for both scenarios one and two. The BER and SNR of the SGD-based ADI mitigation systems were evaluated at the receiver side for different learning rates. The results are presented in Table 28.

In Scenario One, Model 1 achieves a classification accuracy of 0.62 with a learning rate of 0.008, and slightly improves in Scenario Two with an accuracy of 0.65 at a learning rate of 0.012. Precision and recall for Model 1 in both scenarios are moderate, but the F1 scores suggest an imbalance in precision and recall. Model 2 and Model 3 exhibit similar trends, with Model 2 achieving better recall and precision in Scenario Two (0.72 precision, 0.69 recall), while Model 3’s performance is slightly lower overall. Model combinations, such as Models 1 and 2, show improved performance with higher accuracy (0.69), better F1

scores (0.34), and moderate log loss (0.29–0.25), indicating improved model balance and reliability with multiple configurations.

Table 27. The evaluation parameters of the SGD classifier-based ADI mitigation models.

Classifier SGD	Scenario One						Scenarios Two					
	Learning Rate	Test Accuracy	Test Precision	Test Recall	Test F1 Score	Log Loss	Learning Rate	Test Accuracy	Test Precision	Test Recall	Test F1 Score	Log Loss
Model 1	0.008	0.62	0.67	0.69	0.21	0.24	0.012	0.65	0.71	0.62	0.22	0.23
Model 2	0.012	0.61	0.60	0.66	0.22	0.29	0.024	0.61	0.72	0.69	0.21	0.20
Model 3	0.008	0.61	0.61	0.63	0.20	0.28	0.016	0.65	0.68	0.64	0.30	0.25
Model 1 and 2	0.024	0.69	0.68	0.68	0.34	0.29	0.028	0.68	0.66	0.69	0.32	0.25
Model 2 and 3	0.028	0.70	0.65	0.69	0.25	0.23	0.032	0.69	0.71	0.62	0.21	0.25

Table 28. The Bit Error Rates of the SGD classifier-based mitigation systems with different learning rates.

Classifier SGD	BER						SNR					
	Learning Rate		Conventional Configuration Approach		Extended Configuration Approach		Learning Rate		Conventional Configuration Approach (dB)		Extended Configuration Approach (dB)	
	Dataset Is Collected from All the 10 Base Stations	Dataset Is Collected from Only One Base Station	Dataset Is Collected from All the 10 Base Stations	Dataset Is Collected from All the 10 Base Stations	Dataset Is Collected from Only One Base Station	Dataset Is Collected from All the 10 Base Stations	Dataset Is Collected from Only One Base Station	Dataset Is Collected from All the 10 Base Stations	Dataset Is Collected from Only One Base Station	Dataset Is Collected from Only One Base Station	Dataset Is Collected from All the 10 Base Stations	Dataset Is Collected from Only One Base Station
Model 1	0.008	0.012	0.004	0.002	0.004	0.003	0.008	0.012	−11.30	−09.30	−10.30	−10.30
Model 2	0.012	0.024	0.003	0.003	0.003	0.003	0.012	0.024	−10.30	−12.40	−10.10	−12.50
Model 3	0.008	0.016	0.005	0.002	0.004	0.002	0.008	0.016	−11.30	−11.40	−11.20	−11.30
Model 1 and 2	0.024	0.028	0.004	0.002	0.004	0.002	0.024	0.028	−13.20	−10.30	−12.70	−10.40
Model 2 and 3	0.028	0.032	0.002	0.003	0.003	0.003	0.028	0.032	−10.30	−11.20	−11.10	−10.70

In Table 28, the Bit Error Rate (BER) and Signal-to-Noise Ratio (SNR) were evaluated under different learning rates and configurations. The results show that increasing the learning rate leads to a lower BER and an improved SNR, especially in the extended configuration. For instance, in Model 1, the BER decreases from 0.012 to 0.004, and the SNR improves from −11.30 dB to −9.30 dB when using data from all 10 base stations. Similarly, Model 2 shows a reduction in BER (0.003 to 0.002) and an increase in SNR (from −12.40 dB to −10.10 dB) with higher learning rates. The system’s performance improves further with model combinations, particularly in extended configurations, which demonstrate the best error reduction (BER = 0.002) and highest SNR (up to −13.20 dB), suggesting the effectiveness of higher learning rates and extended datasets for mitigating ADI and improving communication quality.

4.2.6. The Results of the HGB Classifier-Based ADI Mitigation System

The results of the HGB classifier-based ADI mitigation system are presented in Table 29, which outlines the evaluation parameters for both Scenario One and Scenario Two. Additionally, the Bit Error Rate (BER) and Signal-to-Noise Ratio (SNR) of the HGB-based ADI mitigation systems were assessed at the receiver side under varying learning rates, with the findings shown in Table 30.

Table 29. The evaluation parameters of the HGB classifier-based ADI mitigation models.

Classifier HGB	Scenario One						Scenarios Two					
	Learning Rate	Test Accuracy	Test Precision	Test Recall	Test F1 Score	Log Loss	Learning Rate	Test Accuracy	Test Precision	Test Recall	Test F1 Score	Log Loss
Model 1	0.004	0.62	0.70	0.67	0.31	0.28	0.024	0.64	0.72	0.62	0.33	0.28
Model 2	0.016	0.62	0.65	0.62	0.35	0.26	0.048	0.61	0.71	0.64	0.29	0.26
Model 3	0.032	0.61	0.66	0.62	0.31	0.18	0.048	0.67	0.72	0.69	0.30	0.10
Model 1 and 2	0.024	0.63	0.69	0.67	0.27	0.21	0.024	0.70	0.61	0.65	0.30	0.24
Model 2 and 3	0.032	0.68	0.69	0.65	0.20	0.23	0.036	0.70	0.70	0.69	0.22	0.12

Table 30. The Bit Error Rates of the HGB classifier-based mitigation systems with different learning rates.

Classifier HGB	BER						SNR					
	Learning Rate		Conventional Configuration Approach		Extended Configuration Approach		Learning Rate		Conventional Configuration Approach (dB)		Extended Configuration Approach (dB)	
	Dataset Is Collected from All the 10 Base Stations	Dataset Is Collected from Only One Base Station	Dataset Is Collected from All the 10 Base Stations	Dataset Is Collected from All the 10 Base Stations	Dataset Is Collected from Only One Base Station	Dataset Is Collected from All the 10 Base Stations	Dataset Is Collected from Only One Base Station	Dataset Is Collected from All the 10 Base Stations	Dataset Is Collected from Only One Base Station	Dataset Is Collected from Only One Base Station	Dataset Is Collected from All the 10 Base Stations	Dataset Is Collected from Only One Base Station
Model 1	0.004	0.024	0.003	0.002	0.004	0.003	0.004	0.024	-11.40	-10.30	-11.30	-09.90
Model 2	0.016	0.048	0.003	0.003	0.003	0.004	0.016	0.048	-10.40	-11.20	-10.40	-11.20
Model 3	0.032	0.048	0.002	0.003	0.002	0.003	0.032	0.048	-10.50	-11.10	-11.20	-11.20
Model 1 and 2	0.024	0.024	0.004	0.005	0.004	0.005	0.024	0.024	-12.40	-13.50	-13.50	-14.40
Model 2 and 3	0.032	0.036	0.003	0.003	0.004	0.003	0.032	0.036	-10.30	-10.40	-10.40	-10.30

In Scenario One, Model 1 achieves an accuracy of 0.62 with a learning rate of 0.004, while in Scenario Two, the accuracy improves slightly to 0.64 when the learning rate is increased to 0.024. Precision values are moderate, ranging from 0.65 to 0.72, with recall varying between 0.62 and 0.67 across different models. Notably, Model 3 shows the best performance in Scenario Two, with the highest recall of 0.72 and precision of 0.71, achieved at a learning rate of 0.048. The combination of Model 2 and Model 3 in Scenario Two performs well, achieving an accuracy of 0.70 with a relatively low log loss of 0.12, suggesting a better balance between precision and recall compared to individual models.

In Table 30, the evaluation of the Bit Error Rate (BER) and Signal-to-Noise Ratio (SNR) reveals the effect of varying learning rates on system performance. As the learning rate increases, the BER consistently decreases, indicating that higher learning rates lead to better error mitigation. For instance, in Model 1, the BER improves from 0.024 to 0.002 when

the learning rate increases. Similarly, the SNR improves with higher learning rates, with Model 1 showing an increase in the SNR from -11.40 dB to -9.90 dB, demonstrating a noticeable enhancement in signal quality. The extended configuration approach generally results in a lower BER and a higher SNR, with Model 2 and Model 3 showing improved performance in Scenario Two, where the SNR reaches -10.30 dB at a learning rate of 0.032. These findings suggest that higher learning rates, especially in extended configurations, lead to more effective ADI mitigation, with improved signal clarity and error reduction.

4.2.7. Discussion: Comparative Analysis of the Six ADI Mitigation Models

In comparing the six ADI mitigation models—GB, LSTM, CNN, ODGB, SGD, and HGB as in Table 31—it becomes evident that LSTM, the CNN, and HGB stand out for their balanced performance across classification and signal quality metrics. LSTM achieved the highest F1 score (0.60) and one of the lowest BER values (0.002), showcasing its effectiveness in both detecting and mitigating interference. The CNN followed closely, excelling particularly in signal clarity, with the highest SNR (-13.7 dB), and HGB offered the best overall classification accuracy (0.70), alongside an F1 score equal to that of LSTM, indicating robustness in diverse deployment scenarios. These three models demonstrate a clear advantage in handling complex, interference-heavy environments typical of TD-LTE networks.

Table 31. The comparative analysis of the ADI mitigation models.

Model Type	Best Accuracy	Best F1 Score	Lowest BER	Highest SNR	Best Ensemble
LSTM	0.68 (M2 + M3)	0.6	0.002	-13.5 dB	M2 + M3
CNN	0.67 (M1)	0.56 (M2 + M3)	0.003	-13.7 dB	M2 + M3
GB	0.66 (M2)	0.36 (M2)	0.002	-13.5 dB	M1 + M2
ODGB	0.68 (M1)	0.7	0.002	-11.8 dB	Mixed
SGD	0.69 (M1 + M2)	0.34	0.002	-13.2 dB	M1 + M2
HGB	0.70 (M2 + M3)	0.70 (M3)	0.002	-10.3 dB	M2 + M3

In contrast, while GB, ODGB, and SGD showed comparatively modest classification capabilities—with lower F1 scores and a slightly higher BER—their performance notably improved with extended configurations and model ensembles. SGD, despite lower classification metrics, achieved a strong SNR (-13.2 dB) and a low BER (0.002), suggesting its suitability for scenarios prioritizing signal recovery over detection precision. Across all models, extended configurations consistently improved the BER and SNR, highlighting the importance of leveraging broader data inputs and ensemble strategies. Ultimately, deep learning models like LSTM and the CNN are best suited for environments where accuracy and adaptability are paramount, while Gradient Boosting and SGD models offer efficient alternatives for more interpretable or lightweight implementations.

5. Conclusions

In this study, we developed and validated an integrated framework for both predicting and mitigating atmospheric duct interference (ADI) in TD-LTE networks—thereby directly addressing two critical research gaps identified in the literature: low prediction accuracy and limited mitigation efficiency.

For the prediction component, we implemented and compared four machine learning algorithms trained on atmospheric and network-side features. The Random Forest model outperformed its peers, achieving a 72.3% accuracy rate—representing a marked improvement over previously reported benchmarks in ADI forecasting. By demonstrating that ensemble methods can robustly capture the complex relationships between meteorological variables and interference events, we have closed a key gap in reliable ADI prediction.

However, to further improve predictive accuracy—particularly under highly variable conditions—future work could explore the integration of temporal modeling techniques such as attention mechanisms or transformer-based architectures, which may offer a more nuanced understanding of the sequential nature of atmospheric phenomena.

On the mitigation side, we introduced a novel, prediction-driven strategy that dynamically configures and de-configures special TD-LTE subframes in real time. Six classification models informed these subframe adjustments, and the LSTM-based approach achieved the highest F1 score (0.60), while the CNN model delivered the highest signal quality, reaching an SNR of -13.7 dB and a BER as low as 0.003. The HGB model further attained the highest classification accuracy (0.70) among all models. These results not only surpass the efficiency of earlier, static mitigation schemes but also highlight the power of combining deep learning with protocol-level adaptations—a hybrid solution that effectively bridges the divide between prediction and action.

While our framework substantially advances the state of the art, we acknowledge that inter-cell and intra-cell interference measurements at the receiver remain unavailable. Incorporating these additional interference metrics into future model feature sets promises to further boost both prediction fidelity and mitigation precision.

Overall, by elevating both predictive performance and mitigation effectiveness, this work lays a solid foundation for next-generation ADI management in wireless systems. The methodologies and promising results detailed here are directly applicable to ongoing research and can inform practical deployments within academic and telecommunications industry contexts.

For future work, we recommend analyzing the performance of the ADI prediction and mitigation models using advanced software tools or APIs. Additionally, we aim to implement these models in hardware, utilizing FPGA or ASIC technologies to bring the framework closer to real-time, scalable deployment in operational networks.

Author Contributions: Conceptualization, U.J. and R.G.R.; methodology, U.J. and R.M.; software, R.M.; validation, R.M., U.J. and R.G.R.; formal analysis, R.M.; investigation, R.M. and U.J.; resources, U.J. and R.G.R.; data curation, R.M.; writing—original draft preparation, R.M. and U.J.; writing—review and editing, U.J., G.M.L. and R.G.R.; visualization, R.M.; supervision, U.J.; project administration, G.M.L.; funding acquisition, G.M.L. All authors have read and agreed to the published version of the manuscript.

Funding: This research received no external funding.

Data Availability Statement: The datasets presented in this article are not publicly available due to a non-disclosure agreement with Dialog Axiata PLC, Sri Lanka. Requests for access to the datasets should be directed at the same.

Acknowledgments: We would like to thank Dialog Axiata, PLC, Sri Lanka, and the Visual Crossing weather monitoring station for providing the dataset to conduct this research.

Conflicts of Interest: The authors declare no conflict of interest.

References

1. Liu, F.; Pan, J.; Zhou, X.; Li, G.Y. Atmospheric Ducting Effect in Wireless Communications: Challenges and Opportunities. *J. Commun. Inf. Netw.* **2021**, *6*, 101–109. [[CrossRef](#)]
2. Sokolovskiy, S.; Schreiner, W.; Zeng, Z.; Hunt, D.; Lin, Y.-C.; Kuo, Y.-H. Observation, Analysis, and Modeling of Deep Radio Occultation Signals: Effects of Tropospheric Ducts and Interfering Signals. *Radio Sci.* **2014**, *49*, 954–970. [[CrossRef](#)]
3. Zhou, T.; Sun, T.; Hu, H.; Xu, H.; Yang, Y.; Harjula, I.; Koucheryavy, Y. Analysis and Prediction of 100 Km-Scale Atmospheric Duct Interference in TD-LTE Networks. *J. Commun. Inf. Netw.* **2017**, *2*, 66–80. [[CrossRef](#)]
4. Zhang, J.; Wu, Z.; Wang, B.; Wang, H.; Zhu, Q. Modeling Low Elevation GPS Signal Propagation in Maritime Atmospheric Ducts. *J. Atmospheric Sol.-Terr. Phys.* **2012**, *80*, 12–20. [[CrossRef](#)]

5. Ericsson. An Overview of Remote Interference Management. Available online: <https://www.ericsson.com/en/blog/2019/9/overview-of-remote-interference-management> (accessed on 25 May 2025).
6. Wei, T.; Feng, W.; Chen, Y.; Wang, C.-X.; Ge, N.; Lu, J. Hybrid Satellite-Terrestrial Communication Networks for the Maritime Internet of Things: Key Technologies, Opportunities, and Challenges. *IEEE Internet Things J.* **2021**, *8*, 8910–8934. [[CrossRef](#)]
7. Dialog Axiata PLC. 4G Mobile Broadband Coverage Area. Available online: <https://www.dialog.lk/support/coverage> (accessed on 25 May 2025).
8. Peralta, E.; Levanen, T.; Mäenpää, M.; Yuk, Y.; Pedersen, K.; Nielsen, S.; Valkama, M. Remote Interference Management in 5G New Radio: Methods and Performance. *EURASIP J. Wirel. Commun. Netw.* **2021**, *2021*, 45. [[CrossRef](#)]
9. Yang, K.; Wu, Z.; Guo, X.; Wu, J.; Cao, Y.; Qu, T.; Xue, J. Estimation of Co-Channel Interference between Cities Caused by Ducting and Turbulence. *Chin. Phys. B* **2022**, *31*, 024102. [[CrossRef](#)]
10. Peralta, E.; Maenpaa, M.; Levanen, T.; Yuk, Y.; Pedersen, K.; Nielsen, S.; Valkama, M. Reference Signal Design for Remote Interference Management in 5G New Radio. In Proceedings of the 2019 European Conference on Networks and Communications (EuCNC), Valencia, Spain, 18–21 June 2019; pp. 559–564. [[CrossRef](#)]
11. Guo, B.; Zhang, L.; Guo, J.; Shen, J.; Fang, Y.; Zhang, Y. Atmospheric Duct Interference Identification and Avoidance in NR TDD Network. In *Signal and Information Processing, Networking and Computers; Lecture Notes in Electrical Engineering; Springer Nature: Singapore, 2024; Volume 1188, pp. 276–284, ISBN 978-981-97-2123-8.* [[CrossRef](#)]
12. Shen, A.; Zhang, Y.; Guo, B.; Wang, G.; Gao, Y.; Liu, J.; Liu, D.; Liu, Y.; Hu, X.; Xie, T. Monitoring and Avoidance of Atmospheric Duct on Interference Optimization in TD-LTE System. In *Signal and Information Processing, Networking and Computers; Lecture Notes in Electrical Engineering; Springer: Singapore, 2018; Volume 473, pp. 36–45, ISBN 978-981-10-7520-9.* [[CrossRef](#)]
13. Ren, J.; Zhang, X.; Xin, Y. Using Deep Convolutional Neural Network to Recognize LTE Uplink Interference. In Proceedings of the 2019 IEEE Wireless Communications and Networking Conference (WCNC), Marrakesh, Morocco, 15–18 April 2019; pp. 1–6. [[CrossRef](#)]
14. Sun, T.; Zhou, T.; Xu, H.; Yang, Y. A Random Forest-Based Prediction Method of Atmospheric Duct Interference in TD-LTE Networks. In Proceedings of the 2017 IEEE Globecom Workshops (GC Wkshps), Singapore, 4–8 December 2017; pp. 1–6. [[CrossRef](#)]
15. Shen, J.-H.; Liu, J.-X.; Zuo, J.-L.; Ding, W.-B.; Shen, A.; Fang, Y.; Zhang, Y.; Wang, X.-D.; Luo, F. Recognition and Optimization of Atmospheric Duct in TD-LTE System Based on Convolutional Neural Network. In Proceedings of the 2020 IEEE Intl Conf on Parallel & Distributed Processing with Applications, Big Data & Cloud Computing, Sustainable Computing & Communications, Social Computing & Networking (ISPA/BDCLOUD/SocialCom/SustainCom), Exeter, UK, 17–19 December 2020; pp. 1389–1393. [[CrossRef](#)]
16. Yang, K.; Guo, X.; Wu, Z.; Wu, J.; Wu, T.; Zhao, K.; Qu, T.; Linghu, L. Using Multi-Source Real Landform Data to Predict and Analyze Intercity Remote Interference of 5G Communication with Ducting and Troposcatter Effects. *Remote Sens.* **2022**, *14*, 4515. [[CrossRef](#)]
17. Zhou, Y.; Samiee, A.; Zhou, T.; Jalali, B. Deep Learning Interference Cancellation in Wireless Networks. *arXiv* **2020**. [[CrossRef](#)]
18. Yang, K.; Wu, Z. Analysis of the Co-Channel Interference Caused by Atmospheric Duct and Tropospheric Scattering. In Proceedings of the 2018 12th International Symposium on Antennas, Propagation and EM Theory (ISAPE), Hangzhou, China, 3–6 December 2018; pp. 1–4. [[CrossRef](#)]
19. Tanveer, J.; Haider, A.; Ali, R.; Kim, A. Machine Learning for Physical Layer in 5G and beyond Wireless Networks: A Survey. *Electronics* **2021**, *11*, 121. [[CrossRef](#)]
20. Zhang, H.; Zhou, T.; Xu, T.; Wang, Y.; Hu, H. FNN-Based Prediction of Wireless Channel with Atmospheric Duct. In Proceedings of the ICC 2021—IEEE International Conference on Communications, Montreal, QC, Canada, 14–23 June 2021; pp. 1–6. [[CrossRef](#)]
21. Pedersen, K.; Esswie, A.; Lei, D.; Harrebek, J.; Yuk, Y.; Selvaganapathy, S.; Helmers, H. Advancements in 5G New Radio TDD Cross Link Interference Mitigation. *IEEE Wirel. Commun.* **2021**, *28*, 106–112. [[CrossRef](#)]
22. Feilong, Z. Forming Interference of Atmospheric Duct in 5G and Avoid Method. *Chin. J. Radio Sci.* **2021**, *36*, 109–115. [[CrossRef](#)]
23. Dinc, E.; Akan, O. Beyond-Line-of-Sight Communications with Ducting Layer. *IEEE Commun. Mag.* **2014**, *52*, 37–43. [[CrossRef](#)]
24. Zhao, X.; Huang, J.; Gong, S. Modeling on Multi-eigenpath Channel in Marine Atmospheric Duct. *Radio Sci.* **2009**, *44*, 1–5. [[CrossRef](#)]
25. Sun, H.; Chen, X.; Shi, Q.; Hong, M.; Fu, X.; Sidiropoulos, N.D. Learning to Optimize: Training Deep Neural Networks for Interference Management. *IEEE Trans. Signal Process.* **2018**, *66*, 5438–5453. [[CrossRef](#)]
26. Gandhi, R. Support Vector Machine—Introduction to Machine Learning Algorithms. Available online: <https://towardsdatascience.com/support-vector-machine-introduction-to-machine-learning-algorithms-934a444fca47/> (accessed on 25 May 2025).
27. Zhang, C.; Zhang, W.; Wang, W.; Yang, L.; Zhang, W. Research Challenges and Opportunities of UAV Millimeter-Wave Communications. *IEEE Wirel. Commun.* **2019**, *26*, 58–62. [[CrossRef](#)]

28. Qian, Y. Integrated Terrestrial-Satellite Communication Networks and Services. *IEEE Wirel. Commun.* **2020**, *27*, 2–3. [[CrossRef](#)]
29. Wang, Y.; Chen, Y.; Zhou, T.; Hu, H. A Traceable Approach to Remote Interference Management for New Radio. In Proceedings of the 2019 IEEE International Conference on Communications Workshops (ICC Workshops), Shanghai, China, 20–24 May 2019; pp. 1–6. [[CrossRef](#)]

Disclaimer/Publisher’s Note: The statements, opinions and data contained in all publications are solely those of the individual author(s) and contributor(s) and not of MDPI and/or the editor(s). MDPI and/or the editor(s) disclaim responsibility for any injury to people or property resulting from any ideas, methods, instructions or products referred to in the content.